Available online at www.sciencedirect.com

ScienceDirect

journal homepage: www.elsevier.com/locate/he

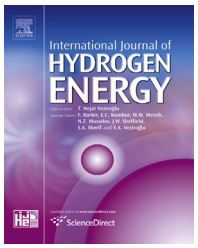

Enhancing triple-phase boundary at fuel electrode of direct carbon fuel cell using a fuel-filled ceria-coated porous anode

*Chengguo Li, Eun Kyung Lee, Yong-Tae Kim, Donggeun Lee**

School of Mechanical Engineering, Pusan Clean Coal Center, Pusan National University, Busan 609-735, South Korea

ARTICLE INFO

Article history:
Received 15 March 2014
Received in revised form
6 August 2014
Accepted 11 August 2014
Available online 5 September 2014

Keywords:
Direct carbon fuel cell (DCFC)
Triple-phase boundary
Porous electrode
Ceria coating

ABSTRACT

A new type of high-temperature fuel cell using solid carbon as a fuel, which is called a direct carbon fuel cell (DCFC), recently attracts scientific and industrial attention due to its excellent electrochemical efficiency, less production of CO_2, and no need of CO_2 separation. However, the state-of-the-art technology on the DCFC still stays in an idea developing stage, mainly because of fuel-related difficulties: a discontinuous fuel supply and a very limited formation of triple phase boundary. In this study, we focused on how to enhance the formation of triple phase boundary at the fuel electrode: using a porous Ni anode filled with carbon particles to enhance the fuel-electrode physical contact and making the porous anode wettable by ceria coating the anode. We demonstrated for the first time that the two ideas are quite successful, leading to 700% increase in a maximal power density and 500% increase in a maximal current density with respect to the standard case.

Introduction

A direct carbon fuel cell (DCFC) that uses carbon-rich solid materials as a fuel produces electricity while releasing CO_2 as a by-product. Despite this release of CO_2, DCFC is more environmental friendly than traditional carbon burning technologies. Due to its highest theoretical efficiency near 100%, DCFC requires less carbon to produce the same amount of electricity. Because only CO_2 is emitted, CO_2 separation from a flue gas in a conventional power station is not necessary. Also used is any form of carbon-containing materials such as carbon black, coals, biomass, and even industrial wastes [1]. Its potential advantages have led to DCFC gaining much more attention.

Many researches for the DCFCs have been performed in a way to modify the fuel electrode of the fuel cells using gaseous fuels for the use of various solid fuels. For example, a cylindrical carbon rod has been inserted in a molten electrolyte pool, in an attempt to use as a solid fuel and an anode [2–4]. Though the overall simplicity in design makes it commercially attractive, there exist a few drawbacks: a surface-limited triple-phase boundary, discontinuous (manual) refueling, and a possible oxidative (rather than electrochemical) consumption of the electrode by dissolved air. Cooper et al. [5–7] in LLNL developed a tilted DCFC system capable of continual refueling with the carbonate-carbon slurry flowing down on the anode. They have also designed a self-feeding cell incorporating pneumatic refueling and internal pyrolysis of the coal [5]. Though they resolved the issue of continuous fuel supply, the

* *Corresponding author.*
E-mail address: donglee@pusan.ac.kr (D. Lee).
http://dx.doi.org/10.1016/j.ijhydene.2014.08.028

electrochemical reaction is constrained on the anode surface. Besides, Vutetakis et al. developed a test bed consisting of a gold working electrode in contact with a coal powder-carbonate slurry, a graphite counter electrode and a gold reference electrode [8]. Though their design enabled to monitor various gas species evolving from the electrochemical reaction [9–11], their cell also suffered from a very limited fuel/electrode/electrolyte contact.

Another type of DCFC was developed on the basis of the solid oxide fuel cell (SOFC). Typical operation temperature of this system is 800–1000 °C, higher than that of the molten carbonate (MC)-based DCFC, although there is a strong technology push to lower the temperature. Note that at such a high temperature, the carbon fuel is not only reacted electrochemically with oxygen ions at the anode ($C + 2O^{2-} = CO_2 + 4e^-$) but also gasified into CO through reverse Boudouard reaction ($C + CO_2 = 2CO$) followed by the electrochemical oxidation of CO ($2CO+2O^{2-} = 2CO_2 + 4e^-$). While the former route requires a direct fuel/electrode/electrolyte contact to be present, the latter does not require so that carbon fuels can be supplied with fluidized or packed beds or even be in a small distance from the anode. Despite this facile fuel supply in this system, it is well known that the CO as an electrochemical reactant reduces the theoretical efficiency and fuel utilization as compared to the direct route. Moreover, the indirect route was not originally aimed in the DCFC system, but rather classified to another fuel reforming version of the SOFC.

Hence, we turned our attention back to the direct route which becomes more probable at temperatures below 700 °C where the reverse Boudouard reaction is thermodynamically inhibited. Overall, it is summarized that the current DCFC technology utilizing the direct anodic reaction of carbon to CO_2 suffers from a discontinuous fuel supply and a limited formation of triple phase boundary. Owing to the triple-phase boundary issue associated with its uneasy handling of solid fuels, the power density of the DCFC is still much lower than that of gas-fueled MCFC or SOFC, making the relevant researches remain in an idea-developing stage or feasibility test level. Despite a large number of relevant papers, there are very few papers attempting to increase the triple phase boundary in the DCFC anode. To the best of our knowledge, only one paper [12] reported that a porous cathode was tested to enhance the cathodic reaction ($2CO_2 + O_2 + 4e^- = 2CO_3^{2-}$). However the result is not quite satisfactory, reporting a maximum power density of ~30 mW cm^{-2} at a current density of 50 mA cm^{-2}.

Thus, this study was focused on enhancing the triple phase boundary at the anode of a MC-based DCFC and demonstrating its effect on the power generation. A porous nickel anode filled with carbon powder was first tested in comparison with a reference case in which carbon powder was put on top of the electrode. Another porous nickel anode was coated with ceria in order to make the electrode electrolyte-wettable and to improve triple phase boundary further. Using a coin-type DCFC cell, it was demonstrated that these ideas are so effective that the electrical power of the cell was increased finally by a factor of seven.

Experimental section

Fig. 1 shows a schematic drawing of a DCFC system for evaluation of a coin-type unit cell. The coin cell comprised a porous Ni anode (INCOFOAM®, porosity 97%), a thin-plate NiO cathode, two sheets of Pt current collectors, and a molten two-component electrolyte sandwiched with two sheets of ceramic matrices which electrically insulated the two electrodes. Detail specifications of the components are summarized in Table 1. Three different modifications of the fuel-anode assembly were considered in a way that investigated the influences of triple-phase boundary and wettability of the

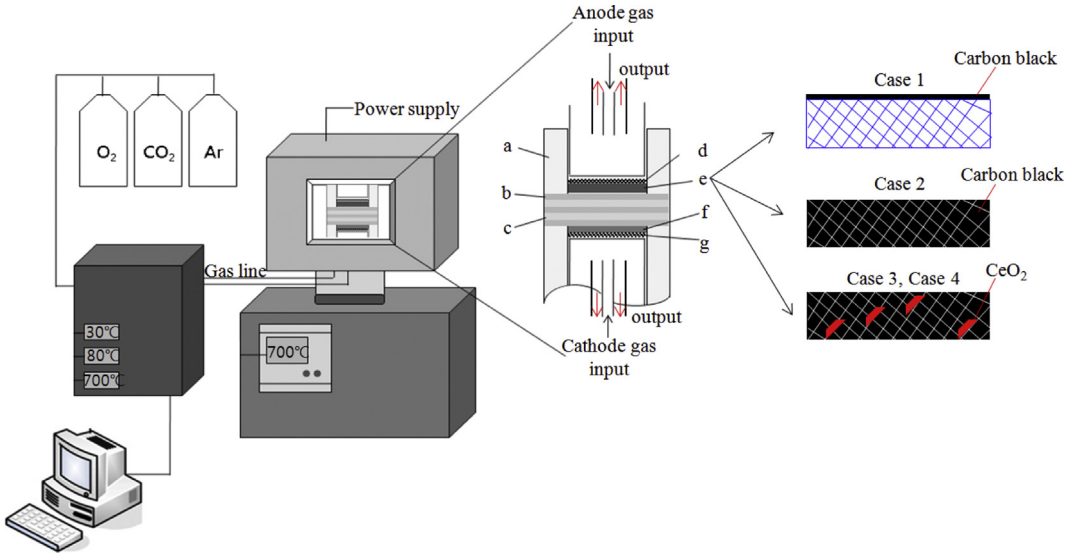

Fig. 1 – Schematics of the present direct carbon fuel cell comprising a) ceramic tube, b) matrix, c) electrolyte, d) anode current collector, e) anode, f) cathode, g) cathode current collector; case 1) putting carbon fuel on top of the porous nickel electrode, case 2) carbon fueling inside the porous nickel electrode, cases 3) and 4) coating the nickel electrode with CeO_2 at two different contents.

Table 1 – Specifications of components for the coin-type cell of the DCFC.

Component	Specification	
Anode	Material	Ni
	Thickness	2.0 mm
	Diameter	1.7 cm
	Current collector	Pt mesh
Cathode	Material	NiO
	Thickness	0.65 mm
	Diameter	1.9 cm
	Current collector	Pt mesh
Matrix	Material	$LiAlO_2$
	Thickness	0.33 mm
	Diameter	2.85 cm
Electrolyte	Material	38 mol%Li_2CO_3–62 mol%K_2CO_3

electrolyte on the anode. As the first case (Case 1 in Fig. 1), a commercial powder of carbon black (Alfa; Purity 99.9%) with 70 nm in diameter weighing 0.5 g was simply placed on top of the porous Ni anode, corresponding to the minimal physical contact between the fuel and electrode. In Case 2, internal porous region of the anode was filled with the same amount of carbon powder to increase such a physical contact as follows. A 0.5 g of carbon powder was first well dispersed in a 50 ml ethanol with a 1-h ultrasonication. The carbon-ethanol slurry was pipetted on top of the porous anode and the bottom surface of the anode was vacuumed. It was confirmed that only pure ethanol was leaked out whereas carbon powder remained inside the anode. This carbon feeding process was repeated until the slurry was consumed completely and then the carbon-containing electrode was dried at room temperature for 24 h. In Case 3, the same carbon treatment as in Case 2 was repeated however to a CeO_2 coated porous Ni anode. The coating of CeO_2 was made in an attempt to improve the electrolyte wettability of the anode in a way that pumps the molten electrolyte up to the anode through the matrix. All the components were tightly fastened in a ceramic tube the both ends of which were blocked with two circular quartz lids. Alumina tubes of 6 mm in diameter were connected to the lids for gas supply. The entire unit cell assembly was kept inside a home-made box furnace during the performance test.

The temperature of the cell in the furnace was raised to a working temperature of 700 °C at a rate of 5 °C min^{-1}. When the cell temperature reached 350–400 °C, CO_2 gas was set to flow to the anode and the cathode at rates of 65 ml min^{-1} and 50 ml min^{-1}, respectively. The purpose of CO_2 supply to the anode was to minimize the evaporation/decomposition loss of the molten carbonate electrolyte [13,14]. When the cell temperature increased over 650 °C, the CO_2 gas flow was stopped at the anode and Ar gas was then supplied at the same flow rate. At the cathode, a mixture of O_2 and CO_2 gas with a volume ratio of 3–5 was supplied at a rate of 50 ml min^{-1}. At a constant temperature of 700 °C, the polarization characteristics of the unit cell in terms of either cell voltage versus current or electrical power versus current were recorded with varying the electrical load, running a Potentiostat/Galvanostat analyzer (Kikusui, PLAZ4W) with dynamic galvano mode. On the basis of the cross-sectional area of the electrode, the power and current densities were calculated from the recorded electrical signals.

A sol–gel method was used for CeO_2 coating on the anode as follows. A 25 mg of cerium chloride heptahydrate ($CeCl_3 \cdot 7H_2O$, Sigma Aldrich) was dissolved in 50 ml ethanol with addition of a 10 mg of citric acid and then kept stirring at room temperature for 30 min. The Ce content in the solution was estimated to be ~0.01 mol%. The porous Ni anode was then dip-coated in the solution and dried at 60 °C in an oven for 1 h. As-prepared anode was calcined under Ar flow for 10 min at 500 °C, leading to formation of CeO_2 coating on the surface, which was labeled as Case 3. Scanning electron microscopy (SEM; S-4800, Hitach, 10 kV) equipped with energy dispersive spectrometer (EDS) was used to explore the microstructural dispersion of the CeO_2 coating on the porous Ni anode.

Though measuring contact angle of a solvent drop on a substrate is a well known technology to determine a solvent affinity of the substrate, it is almost impossible to form a distinct hemispherical droplet on a porous substrate. Thus, a Ni flat plate was alternatively used for the measurement of the contact angle as follows. A scoop of pristine electrolyte powders, weighing 95 mg, was put on a flat surface of Ni plate and then heated at 520 °C in a tube furnace (w/30 cm-long hot

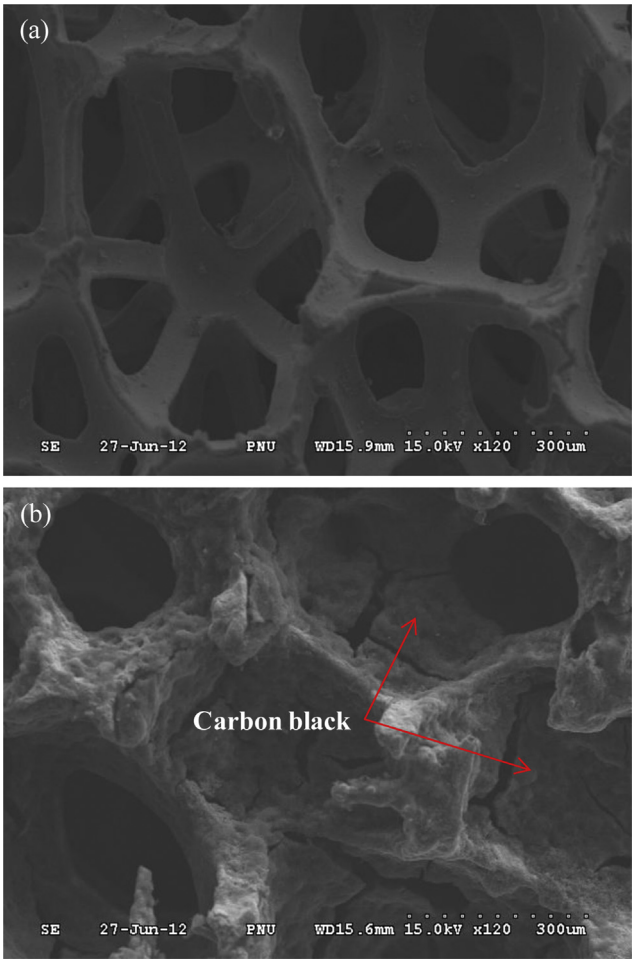

Fig. 2 – SEM images of a) bare porous nickel anode and b) the same anode filled with carbon particles.

zone) in Ar atmosphere until the scooped electrolyte was completely melted to form a hemispherical shape. Then the furnace was quenched by flowing air at 50 l pm. As-received hemispherical electrolyte solid on top of the Ni plate was imaged to measure the contact angle between electrolyte and Ni plate using a contact angle analyzer (Phoenix 300, Kr).

Results and discussion

As shown in Fig. 2(a), the porous Ni anode used in this study exhibits three-dimensional porous structure with internal pores of ~120 μm, looking like being woven of ~60 μm Ni wires. Carbon feeding process corresponding to Case 2 was performed inside the porous Ni anode. Fig. 2(b) shows a resultant internal structure of the anode in which carbon black powder were evenly dispersed on the surface of the anode. As such, the physical contact between the anode and fuels becomes quite certainly enhanced with respect to Case 1 in Fig. 1. However, as aforementioned in Chap. 2, there is another hurdle to overcome: insufficient electrolyte supply to the fuel-anode contact resulting from the non-wetting nature of the Ni anode and/or pyrolytic loss of the molten electrolyte at high temperature [15–17].

To meet this challenge, the ceria coating was made on the porous Ni anode according to Case 3 and its SEM image was shown in Fig. 3(a). As compared to Fig. 2(a) showing the bare Ni electrode with smoother surface, a lot of white polygonal fragments are newly formed on the electrode, probably resulting from the ceria coating. A part of white coating fragments marked with a circle in Fig. 3(a) was chemically analyzed using EDS elemental mapping and the result is shown in Fig. 3(a1). Blue, green, and red dots represent cerium, oxygen, and nickel, respectively. It is no doubt that the white polygonal fragments are CeO_2 coatings while the surroundings are mainly metallic Ni electrode containing fewer tiny CeO_2 dots. For comparison, the Ce content in the solution was increased by a factor of 10, i.e., to ~0.1 mol % and then subjected to the same treatment for ceria coating. This is referred to as Case 4. Fig. 3(b and b1) show that thicker and wider CeO_2 coating layers are distinctively produced.

Next is to investigate the nature of electrolyte-electrode affinity and the effect of ceria coating on it. Fig. 4(a) shows a hemispherical part of molten carbonate resting on top of a flat plate of nickel, measuring a contact angle of 101.5°. As expected, the carbonate electrolyte is mostly non-wetting the Ni electrode. However, a small amount of CeO_2 coating generates a dramatic change in the electrolyte affinity as seen in Fig. 4(b): the droplet of molten electrolyte spreads almost completely, resulting in a contact angle of 29.5°. Denser coating of CeO_2 in Case 4 further decreases the contact angle to 20.4°, suggesting that the ceria coating progressively improve the electrolyte affinity of Ni anode. It might be concluded that the present approaches corresponding to Case 2 & Case 3 help to realize the conceptual increase of triple phase boundary.

Of particular interest is to explore any difference in electrochemical power generation of Cases 1–4 in a quantitative manner. The cell performance of each case was measured in

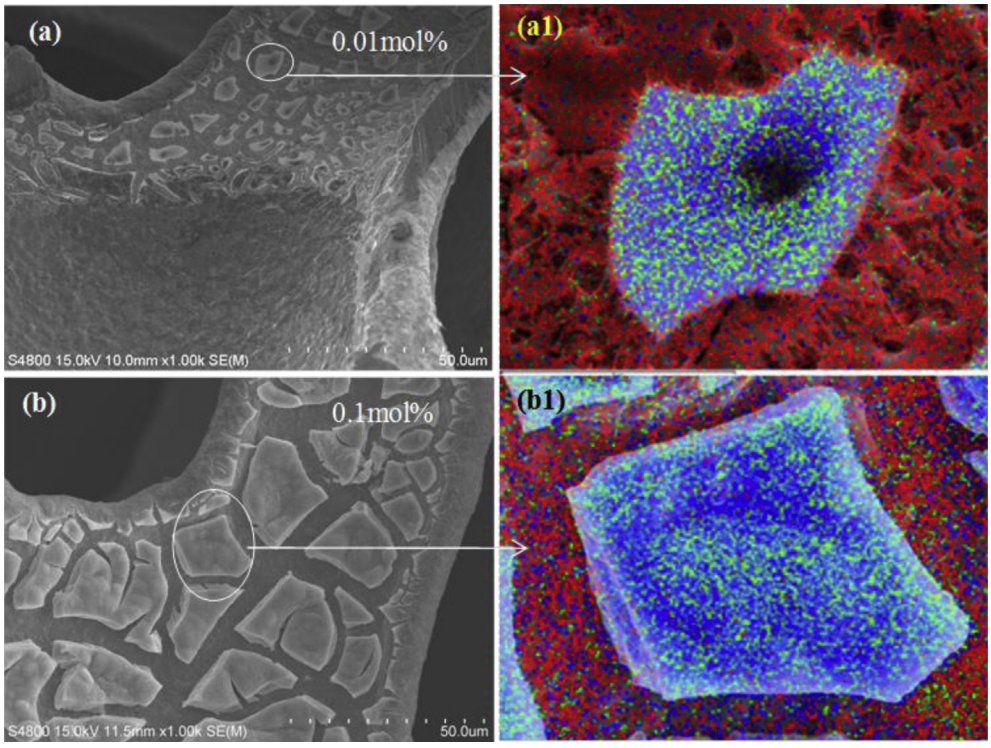

Fig. 3 – Microstructures of the porous nickel electrode coated with CeO_2; a) at a low concentration and b) at a high concentration; colored images of a1) and b1) are elemental mapping results corresponding to a) and b), respectively; blue, green, and red dots represent Ce, O, and Ni, respectively. (For interpretation of the references to color in this figure legend, the reader is referred to the web version of this article.)

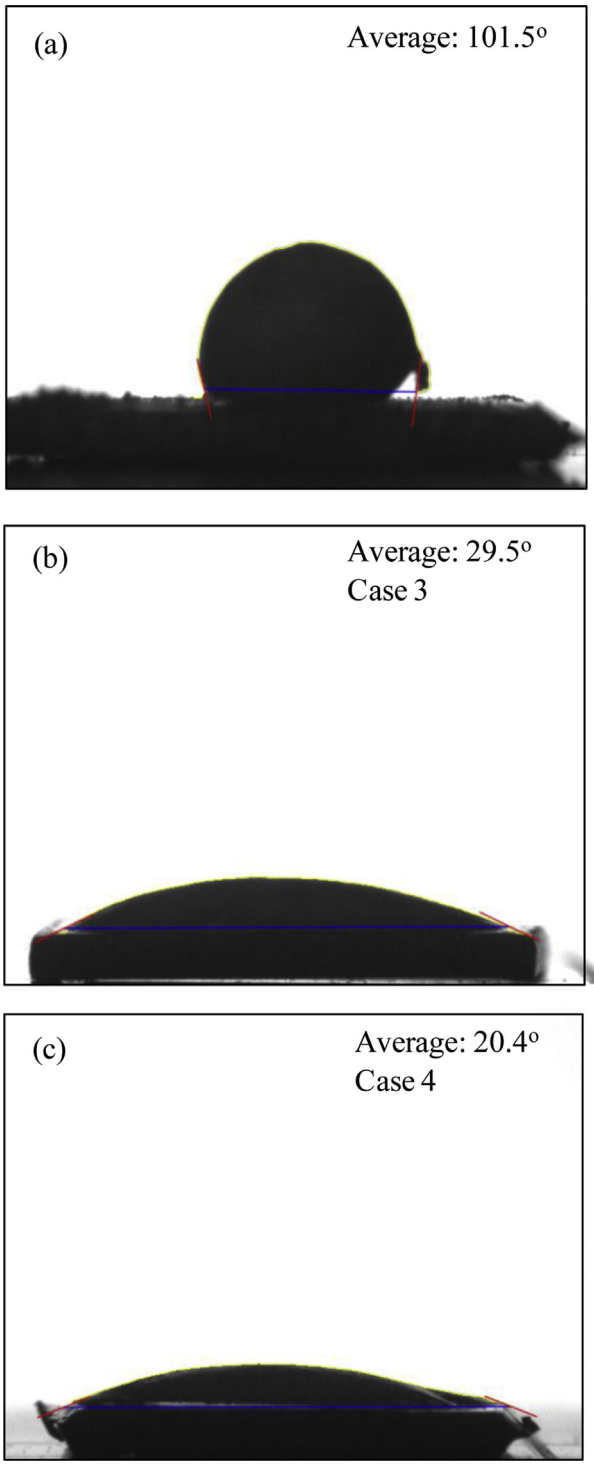

Fig. 4 – Contact angle of a hemispherical molten electrolyte on a) a bare nickel plate and a nickel plate coated with CeO_2 b) at a low concentration and c) at a high concentration.

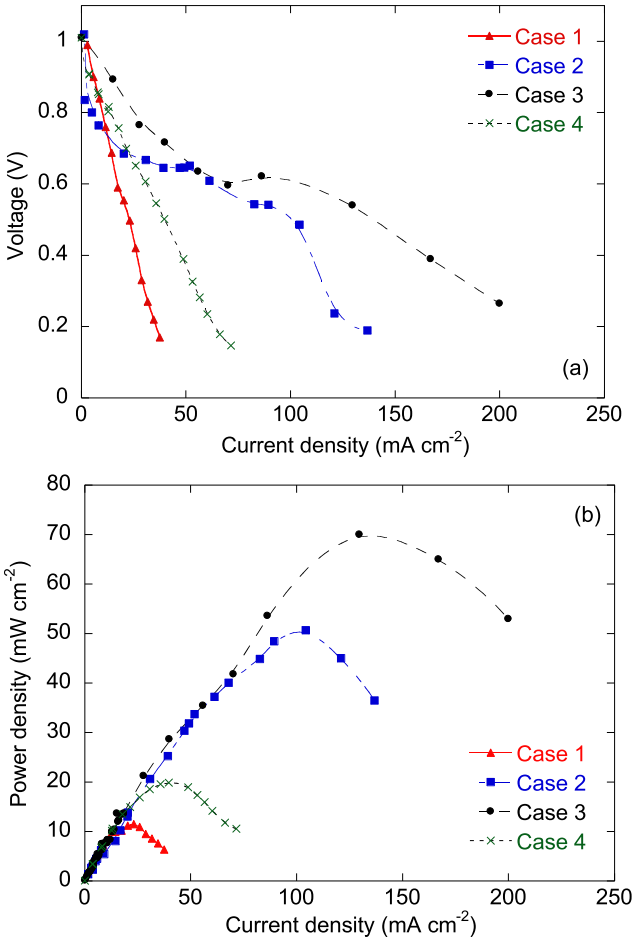

Fig. 5 – Comparisons of the electrochemical performances of the DCFC cells among Cases 1–4; a) electrical voltage versus current density and b) power density versus current density.

terms of electrical voltage and power density as a function of current density as seen in Fig. 5(a and b), respectively. In all cases, open circuit voltage (OCV) of the cell varied from 1.01 V to 1.06 V, almost invariant from a theoretical value[1] of 1.02 V corresponding to the net reaction of $C + O_2 = CO_2$, suggesting that other gaseous reactants such as CO that can increase the OCV did not participate in the reaction especially at the lower current limit. As the current density increased in Case 1, the cell voltage decreased rapidly and almost linearly as if overwhelmed by activation overpotential. When the fuel-electrode contact was improved as in Case 2, however, the polarization curve comprised a nonlinear activation overpotential below the current density of ~30 mA cm^{-2} and a successive pseudo-linear ohmic overpotential or IR-loss up to ~100 mA cm^{-2}. This behavior becomes more pronounced in Case 3. In Case 4, the polarization characteristics returned to Case 1. Note that only anode was modified while other components were not changed. It is thus natural to conjecture that the difference in the polarization curves arises from the modification of the anode. By comparison with Case 2, the rapid voltage drop in Case 1 is attributed to poor activity of the anode which could be improved by increasing physical contact area of fuel and anode. Easy access to the molten electrolyte inside the anode in Case 3 could further improve the anodic activation overpotential and the ohmic loss as well.

In Fig. 5(b), the maximal power density of Case 1 is only 12 mW cm^{-2} at a current density of 20 mA cm^{-2}. Anode treatment in Case 2 results in 500% increase in the maximal

power density as well as 400% increase in the maximal current density. This result clarifies the primary role of the fuel-electrode contact in the power generation: the carbon consumes mainly by the direct electrochemical reaction at the anode ($C + 2CO_3^{2-} = 2CO_2 + 4e^-$), not by the indirect pathway ($C + CO_2 = 2CO$; $CO + CO_3^{2-} = 2CO_2 + 2e^-$) where the carbon-anode contact is not necessarily required. Regarding that the reactant CO_3^{2-} ions in the anodic reaction are transferred only through the ion-conducting electrolyte, it is natural to ascribe the further increase of power density (from Case 2 to Case 3) in Fig. 5(b) to as-aforementioned easy access of carbon to molten carbonate, that is, the better triple phase boundary. It is worth noting that the maximal power density reaches ~70 mW cm^{-2} at ~130 mA cm^{-2} and the maximal value of the current density seemingly exceeds 250 mA cm^{-2}, which is comparable to the world best in DCFC system operating below 700 °C [1]. It is of another interest to observe that the power generation is significantly downgraded upon greater coating of CeO_2 (from Case 3 to Case 4): the maximum power density is only ~20 mW cm^{-2}. A possible explanation came from the fact that most metal oxides are not good conductors for ions and electrons. In other words, too much coating of ceria, despite its further improvement of electrolyte affinity, likely hinders a direct contact of carbon with the electrode, leading to an increase in internal resistance and thereby a big loss in the power generation. This again supports that the present DCFC system works mainly through the direct route of carbon and indicates the significance of the triple phase boundary at least under the present condition. Back in Fig. 5(a), the anodic activation overpotential of ~0.35 V is comparable to ~0.4 V of SARA's MARK II-D DCFC cell working at 630 °C [18], however larger than those of other DCFC working at higher temperatures of 800–930 °C [6,19–21]. Since CO resulting from carbon above 700 °C can reduce the anodic overpotential due to its higher mobility and electrochemical reactivity as compared to carbon, the relatively large value of anodic overpotential in Case 3 implies again that the carbon mainly reacts with the aforementioned direct route in the present condition.

Now, it might be concluded that the fuel-electrode contact is of the greatest significance in determining the cell performance of the DCFC, whereas the electrolyte wettability of the electrode is likely secondary. This is understood because the 500% increase in the power density was achieved only by enhancing the contact whereas the optimal CeO_2 coating leads to the 40% additional increase. Despite the limited contribution of CeO_2 coating, it is of great interest to further study the role of the CeO_2. The CeO_2 coating may interact with Ni supports at high temperature, similar to a strong metal support interaction in heterogeneous catalysts, as described by $CeO_2 + Ni \rightarrow CeO + NiO$. This oxygen exchange interaction can commence another electrochemical reaction of $CeO + CO_3^{2-} \rightarrow CeO_2 + CO_2 + 2e^-$. Since the second reaction producing electricity is restricted by the availability of CeO, an additional experiment has been performed as follows to estimate the extent of the first reaction and relative contribution of the second reaction. A commercial powder of CeO_2 (Aldrich) was well mixed with Ni powder with a weight ratio of 1:1 and then compressed to a pellet. The pellet was then heat-treated at the same condition as in the present DCFC experiment: heating at 700 °C for an hour in a tube furnace, flowing Ar gas. The mixture sample of CeO_2 and Ni, before and after the heat treatment, was characterized with X-ray diffraction (XRD; D/Max-2004, Rigaku) and X-ray photoelectron spectroscopy (XPS; ESCALAB 250 XPS spectrometer).

The XRD measurement was performed by scanning the angle of 2θ in a range of 20°–90° with 4°min^{-1}, while irradiating Cu Kα X-ray (30 kV, 40 mA, 0.15218 nm). Fig. 6 shows XRD profiles of the CeO_2–Ni powder mixture before and after the heat treatment. The pristine sample before the heat treatment, as expected, consists of the CeO_2 and Ni only. After the heating at 700 °C, little peaks of NiO newly appear. For an hour heating (operation of DCFC), the content of NiO increases up to 7% together with almost invariant peaks of CeO_2 and Ni, suggesting that the NiO is apparently not the product of the CeO_2–Ni interaction. There is indeed an alternative route to the NiO not involving CeO_2: since most metals are often covered with thin amorphous oxide (or hydroxide) layers [22], the high-temperature heating of the sample can transform the amorphous part into the crystalline layer.

In order to test this inference, surface species of CeO_2 and Ni were investigated by XPS upon irradiating Al Kα X-ray with a resolution of 0.45 eV. Ni 2p XPS spectra in Fig. 7(a) show that there is a distinct difference in a range of 850–865 eV before and after the heating. Before the heating, the first peak at 853.0 eV is assigned to Ni^{2+} state in an amorphous NiO [23] whereas the second peak at 856.3 eV is assigned to that of $Ni(OH)_2$ [24]. After the heating, the amorphous NiO peak disappears or turns into a huge peak at 855.3 eV representing the crystalline NiO [25]. In addition, Ce XPS spectra in Fig. 7(b) show that nothing happens in surface states of CeO_2 contrary to the CeO_2–Ni interaction. These observations indicate that the CeO_2 does not undergo any (electro)chemical reactions. Furthermore, net reaction of the ceria-involved two step reactions is $Ni + CO_3^{2-} \rightarrow NiO + CO_2 + 2e^-$. This reaction, if happens, keeps (electrochemically) oxidizing the Ni to NiO, just like consuming carbon fuels. Since the Ni is also an electrode, the NiO should be regenerated to Ni for continuing the electricity production. However the NiO regeneration does not occur at 700 °C in the absence of strong reducing gas such

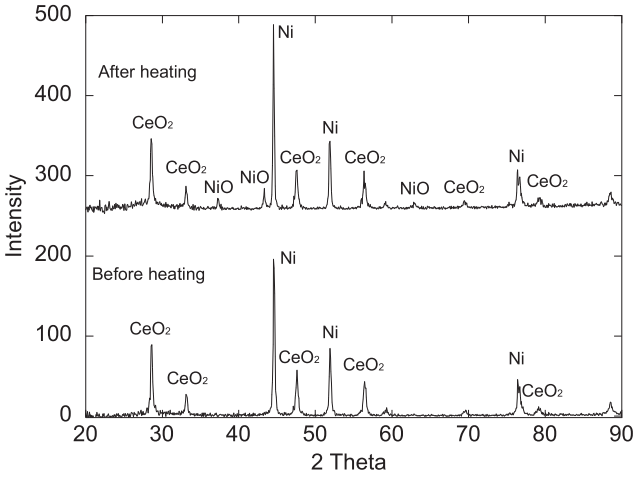

Fig. 6 – Comparisons of XRD profiles of CeO_2–Ni powder mixture before and after heating at the same condition as the current DCFC operation: at 700 °C for 1 h in Ar flow.

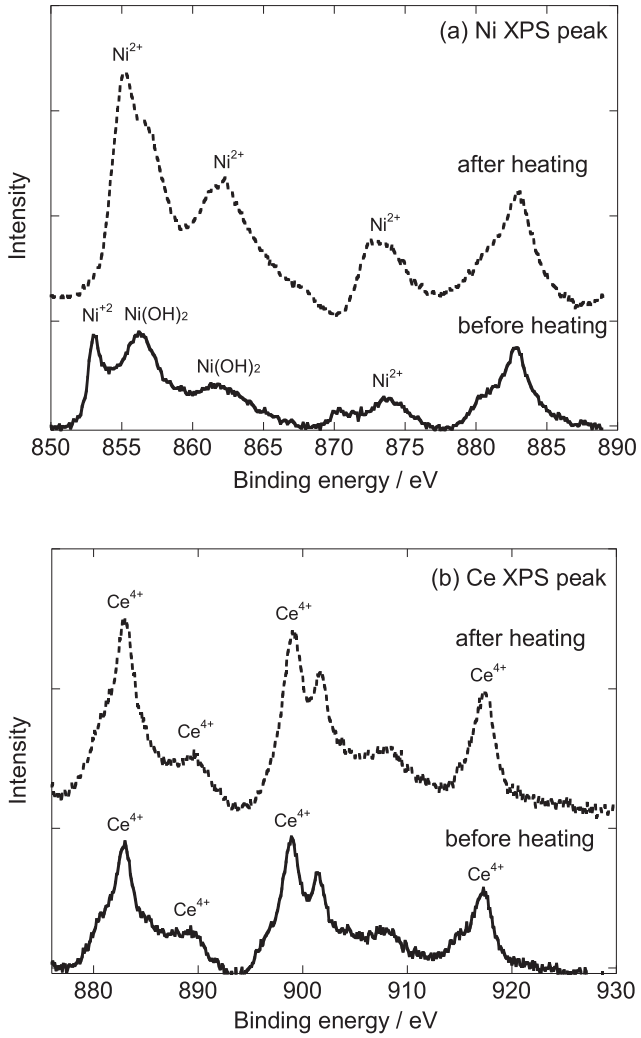

Fig. 7 – Comparisons of XPS spectra of CeO_2–Ni powder mixture before and after heating; a) Ni 2p peaks and b) Ce 3d peaks.

as hydrogen [26]. Overall, all of these results seem to conclude that CeO_2–Ni interaction does not likely occur at least at the current operating condition of the DCFC.

Conclusions

In this work, we proposed a simple idea to enhance the triple phase boundary formation at the fuel electrode of the DCFC and demonstrated for the first time that the physical contact between the solid fuel and electrode plays a key role in the power generation, unlike in the conventional gas-fueled fuel cells. Firstly, a porous Ni anode filled with carbon particles was tested in comparison with the standard case in which carbon powder was put on top of the same anode. Enhancing the physical contact between the fuel and electrode was found to be very effective, leading to a five-fold increase in maximal power density and a four-fold increase in maximal current density. Secondly, the non-wetting Ni anode was coated with CeO_2 in an attempt to attract the molten carbonate electrolyte toward the anode. This approach could enhance the cell performance further by as much as ~40%, up to a maximal power density of ~70 mW cm^{-2} and a maximal current density exceeding ~250 mA cm^{-2}. Too much coating of ceria, despite its further improvement of electrolyte affinity, likely hindered such a direct contact of carbon with the electrode, leading to an increase in internal resistance and thereby a significant loss in the power generation.

Acknowledgments

This work was supported by the National Research Foundation of Korea (NRF) grant funded by the Korea Government (MSIP) (No. 2010-0019543), by the Human Resources Development Program (No. 20124010203230) of the Korea Institute of Energy Technology Evaluation and Planning (KETEP) grant funded by the MOTIE, and also by the Global Frontier R&D Program on Center for Multiscale Energy System funded by the National Research Foundation under the MSIP (No. 2012M3A6A7054863).

REFERENCES

[1] Giddey S, Badwal SPS, Kulkarni A, Munnings C. A comprehensive review of direct carbon fuel cell technology. Prog Energy Combust Sci 2012;38:360–99.
[2] Jacques WW. Method of converting potential energy of carbon into electrical energy. US Patent no. 555, 511, 1896.
[3] Zecevic S, Patton EM, Parhami P. Electrochemistry of direct carbon fuel cell based metal hydroxide electrolyte. Presented in direct carbon fuel cell workshop – NETL, Pittsburg, PA, USA, 30th July, 2003, http://www.netl.doe.gov/publications/proceedings/03/dcfcw/Zecevic.pdf.
[4] Hackett GA, Zondlo JW, Svensson R. Evaluation of carbon materials for use in direct carbon fuel cell. J Power Sources 2007;168:111–8.
[5] Cooper JF, Berner K. Presented in fuel cell seminar, direct carbon fuel cell workshop – Palm Springs, CA, USA, 14th November 2005, Proceedings online: http://www.fuelcellseminar.com/pdf/Direct Carbon Fuel Cell Workshop/Cooper John.pdf.
[6] Cooper JF. Reactions of the carbon anode in molten carbonate electrolyte. Presented in direct carbon fuel cell workshop – NETL, Pittsburg, PA, USA, 30th July, 2003, Proceedings – http//www.netl.doe.gov/publications/proceedings/03/dcfcw/cooper.Pdf.
[7] Cooper JF, Cherepy N, Krueger RL. US patent 2005; No. 6, 878, 479.
[8] Vutetakis DG, Skidmore DR, Byker HJ. Electrochemical oxidation of molten carbonate-coal slurries. J Electrochem Soc 1987;134:3027–35.
[9] Li X, Zhu ZH, De Marco R, Dicks A, Bradley J, et al. Factors that determine the performance of carbon fuels in the direct carbon fuel cell. Ind Eng Chem Res 2008;47:9670–7.
[10] Li X, Zhu ZH, Chen JL, De Marco R, Dicks A, Bradley J, et al. Surface modification of carbon fuels for direct carbon fuel cells. J Power Sources 2009;186:1–9.
[11] Li X, Zhu Z, Marcob RD, Bradleya J, Dicksa A. Evaluation of raw coals as fuels for direct carbon fuel cells. J Power Sources 2010;195:4051–8.
[12] Kouchachvili L, Ikura M. Performance of direct carbon fuel cell. Int J Hydrogen Energy 2011;36:10263–8.

[13] Cao DX, Sun Y, Wang GL. Direct carbon fuel cell: fundamentals and development. J Power Sources 2007;167:250–7.
[14] Lee AC, Mitchell RM, Gur TM. Thermodynamic analysis of gasification-driven direct carbon fuel cells. J Power Sources 2009;194:774–85.
[15] Kim YS, Lee KY, Chun HS. Creep characteristics of porous Ni/Ni_3Al anodes for molten carbonate fuel cells. J Power Sources 2001;99:26–33.
[16] Selman JR, Maru HC, Mamatov G, Braunstein J, Mamantov CB. Advances in molten salt chemistry. ECS 1981;4:182–4.
[17] Ong ET, Claar TD, Selman JR. Proceedings of the symposium on molten carbonate fuel cell technology, 84. Inc Electrochemical Society; 1984. p. 54–80.
[18] Zecevic S, Patton EM, Parhami P. Carbon-air fuel cell without a reforming process. Carbon 2004;42:1983–93.
[19] Hasegawa S, Ihara M. Reaction mechanism of solid carbon fuel in rechargeable direct carbon SOFCs with methane for charging. J Electrochem Soc 2008;155:B58–63.
[20] Gur TM, Homel M, Virkar AV. High performance solid oxide fuel cell operating on dry gasified coal. J Power Sources 2010;195:1085–90.
[21] Lee AC, Li S, Mitchell RE, Gur TM. Conversion of solid carbonaceous fuels in a fluidized bed fuel cell. Electrochem Solid St 2008;11:B20–3.
[22] Firmansyah DA, Sullivan K, Lee KS, Kim YH, Zahaf R, Zachariah MR, et al. Microstructure behavior of the alumina shell and alumina core before and after melting of alumina nanoparticles. J Phys Chem 2012;116:404–11.
[23] Sim JK, Seo HO, Jeong MG, Kim KD, Kim YD, Lim DC. Catalytic NiO filter supported on carbon fiber for oxidation of volatile organic compounds. Bull Korean Chem Soc 2013;34:2105.
[24] Oswald S, Bruckner W. XPS depth profile analysis of non-stoichiometric NiO films. Surf Interface Anal 2004;36:17–22.
[25] Agrawal A, Habibi HR, Agrawal RK, Cronin JP, Roberts DM. Effect of deposition pressure on the microstructure and electrochromic properties of electron-beam-evaporated nickel oxide films. Thin Soild Films 1992;221:239–53.
[26] Firmansyah DA, Kim T, Kim S, Sullivan K, Zachariah MR, Lee D. Crystalline phase reduction of cuprous oxide (Cu_2O) nanoparticles accompanied by a morphology change during ethanol-assisted spray pyrolysis. Langmuir 2009;25:7063–71.